



Regular article

In-situ synchrotron X-ray diffraction study of dual-step strain variation in laser shock peened metallic glasses

Liang Wang^a, Yakai Zhao^a, Lu Wang^{a,b}, Zhihua Nie^a, Benpeng Wang^c, Yunfei Xue^{a,b,*}, Haifeng Zhang^d, Huameng Fu^d, Dennis E. Brown^e, Yang Ren^f^a School of Materials Science and Engineering, Beijing Institute of Technology, Beijing 100081, China^b National Key Laboratory of Science and Technology on Materials under Shock and Impact, Beijing 100081, China^c School of Mechanical Engineering, Beijing Institute of Technology, Beijing 100081, China^d Shenyang National Laboratory for Materials Science, Institute of Metal Research, Chinese Academy of Sciences, Shenyang 110016, China^e Department of Physics, Northern Illinois University, De Kalb, IL 60115, USA^f X-ray Science Division, Argonne National Laboratory, Argonne, IL 60439, USA

ARTICLE INFO

Article history:

Received 11 January 2018

Received in revised form 15 February 2018

Accepted 15 February 2018

Keywords:

Metallic glass

Laser shock peening

In-situ synchrotron X-ray diffraction

Flow unit interconnection

ABSTRACT

Atomic-structure evolution is significant in understanding the deformation mechanism of metallic glasses. Here, we firstly find a dual-step atomic strain variation in laser-shock-peened (LSPed) metallic glasses during compression tests by using in-situ synchrotron X-ray diffraction. Under low compressive load, LSP-deformed zone's atomic-structure shows low Young's Modulus (E); with load increase, atomic-structure are re-hardened, showing high E . An atomic deformation mechanism is proposed by using flow unit model, that LSP could induce interconnected flow units and homogenize the atomic-structure. These interconnected flow units are metastable and start to annihilate during compressive loading, causing the dual-step atomic strain variation.

© 2018 Acta Materialia Inc. Published by Elsevier Ltd. All rights reserved.

Due to the absence of long-range order, bulk metallic glasses (BMGs) exhibit excellent mechanical properties, such as high strength, large elastic strain limit, and high hardness [1,2]. Different from crystalline solids, BMGs do not possess a microstructure with dislocations, twins, or stacking faults. The structural origin of BMG deformation has been investigated for decades but still not fully understood, mainly due to the absence of direct experimental characterization of atomic-structure evolution. High energy synchrotron X-ray diffraction (HESXRD) is an effective tool to explore the details of BMG deformation mechanism in atomic level [3–8]. Poulsen et al. [3] demonstrated that the atomic strain tensor of BMGs could be quantitatively estimated by considering the shift of peak positions of the pair-distribution-function (PDF) curves. Based on this approach, it was found that during elastic deformation in BMGs, the atomic strain in atomic shells varied linearly with the applied stress [4,6–8]; and the bonds in 1st atomic shell are much stiffer against external loading compared to high order shells, showing the structure heterogeneity. However, the atomic-structural evolution in plastic deformed BMG is still unclear. The main reason is that in BMG, the plastic flow usually localizes in nano-scaled shear bands and brittle

fracture happens quickly, the plastic deformation zone is narrow and difficult to be researched experimentally.

Laser shock peening (LSP), which can induce high impact stress ($>10\text{GPa}$) with high strain rate ($>10^6\text{ s}^{-1}$) on materials, is an effective method to induce large plastic deformation zone with high energy in BMGs. Free volume and multiple shear bands can be generated by LSP [9–11]. The deformed zone is obviously softened and the depth is $>500\text{ }\mu\text{m}$ [12,13]. This large plastic deformed zone provides an opportunity to research the structure evolution in plastic deformed MGs directly.

Here, we used LSP to induce intense plastic deformation in Ti-based BMGs. In-situ HESXRD process and PDF analysis were employed to investigate the atomic-structure evolution in LSPed BMGs during compression. We found that not only high-order shells, but also 1st atomic shell were greatly softened. A dual-step atomic strain variation with different Young's Modulus (E_s) in LSPed BMGs was observed during compression tests. By using a flow unit model, an atomic deformation mechanism is proposed, that metastable interconnected flow units were induced by LSP and the structure heterogeneity were weakened. The increase of E in high load region reveals the structure relaxation.

$\text{Ti}_{32.8}\text{Zr}_{30.2}\text{Ni}_{5.3}\text{Cu}_9\text{Be}_{22.7}$ (at.%) BMG plates with dimensions of $50 \times 50 \times 3\text{ mm}^3$ were prepared by flip casting into a copper mold. BMG plates were shocked by laser pulse with wavelength of 1064 nm, the power density of a single laser pulse with 3 mm diameter is

* Corresponding author at: School of Materials Science and Engineering, Beijing Institute of Technology, Beijing 100081, China.

E-mail address: xueyunfei@bit.edu.cn (Y. Xue).

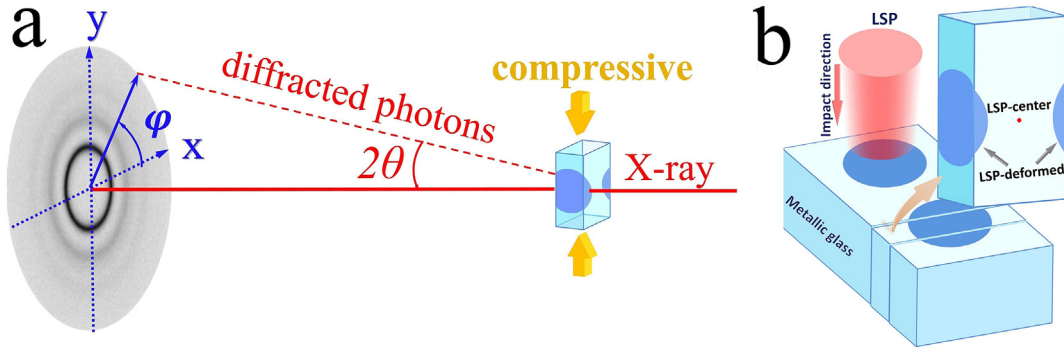


Fig. 1. The schematic diagram of the HESXRD measurement (a) and sample preparation (b).

25 GW/cm² and the pulse duration is 30 ns (see details in supplementary material). In-situ HESXRD technique was used to study the atomic-structural evolution of LSPed BMG at the 11-ID-C beamline of Advanced Photon Source, Argonne National Laboratory, USA. The process of the measurement is schematically shown in Fig. 1a. For the LSPed sample, plastic deformed zone and center zone (referred as LSP-deformed and LSP-center, respectively, as illustrated in Fig. 1b) were select to be measured by HESXRD. Based on the XRD patterns, the reduced pair distribution function (PDF), $G(r)$, were calculated using the software package of Fit2D [14] and PDF getX2 [15] (see HESXRD measurement and PDF analysis details in supplementary material).

Fig. 2a presents the reduced PDFs, $G(r)$, of the as-cast BMG, LSPed BMG samples before loading ($\sigma = 0$ MPa). The inset of Fig. 2a shows that the first peak of $G(r)$ shifts to lower r after LSP, indicating that the 1st atomic shell in BMGs was obviously compressed.

The isotropic atomic packing structure of BMGs can become anisotropic under loading [5], and the atomic strain ε_i of the i th atomic shell caused by the applied stress σ can be calculated according to the following eq. [4]:

$$\varepsilon_i(\varphi) = \frac{r_i(0, \varphi) - r_i(\sigma, \varphi)}{r_i(\sigma, \varphi)} \quad (1)$$

The angular variation of strain can be fitted to the following expression [4]:

$$\varepsilon_i(\varphi) = \varepsilon_{ix} \sin^2 \varphi + \gamma_{ixz} \sin \varphi \cos \varphi + \varepsilon_{iz} \cos^2 \varphi \quad (2)$$

Fig. 2b shows the atomic strain distribution in different directions (φ s, as shown in Fig. 1a) of LSP-deformed before loading. The strain distribution of the 1st atomic shell has a good consistency with that of the 3rd atomic shell, indicating a similar mechanical response to LSP process shared by the 1st and the 3rd atomic shells. The inhomogeneous strain distribution reveals that LSP induced anisotropic residual stress in the BMG sample [12], leading to the anisotropic atomic packing [8].

To analyze the LSPed atomic-structure evolution in compression tests, atomic strain variation along the compressive loading direction ($\varphi = 90^\circ$) in the as-cast BMG, LSP-center, and LSP-deformed zone are extracted and compared, the 1st shell strain results are shown in Fig. 2c. For the as-cast BMG and LSP-center, the atomic strain varies linearly with the stress, which agrees well with previous studies [4,6–8]. However, the strain variation in LSP-deformed zone is quite complicated. Firstly, the initial strain of LSP-deformed is not 0, showing the residual strain in 1st shell. Secondly, dual-step variation with inflection point at $\sigma_i \approx 400$ MPa was observed during compressive loading (hereafter $\sigma < 400$ MPa is called step A and $400 \text{ MPa} < \sigma < 1200$ MPa is called step B), indicating that an atomic-structure transformation appears around 400 MPa. When the applied stress $\sigma > 1200$ MPa, the atomic strain became constant, and the BMG structure yielded [8]. Young's modulus E can be estimated from the slope of the stress-strain curves in Fig. 2c, and the results are presented in the inset of Fig. 2c. Compared with as-cast sample, E values of the LSP-center and the step A of LSP-deformed zone are much lower, indicating that the LSP process clearly decreases the atomic bond strength [16] and softens the atomic-structure. Such softening in LSP-center shows that LSP could change BMG structure as deep as 1500 μm . In step B, the E recovered, suggesting the re-hardening of the structure.

Moreover, in as-cast BMG and LSP-center, the higher stress-strain curve slope of 1st shell than that of 3rd shell (shown in Fig. S2a and S1b) indicates that 1st shell is stiffer than 3rd shell. This phenomenon demonstrates the structure heterogeneity. However, in LSP-deformed zone, there is some overlap of the stress-strain curves between 1st shell and 3rd shell (shown in Fig. S2c), showing the similar E s in 1st and 3rd shell. Combined with the similar residual strain distribution between 1st shell and 3rd shell in LSP-deformed zone (Fig. 2b). We found that LSP process clearly weakened the structural heterogeneity between the 1st shell and high order shells, indicating an atomic-structural homogenization in BMG. To further understand the atomic-structural homogenization and the mechanism of the dual-step atomic strain variation in LSP-deformed zone, the flow units, which could be regarded as the basic deformation units in MGs [17–19], is necessary to be

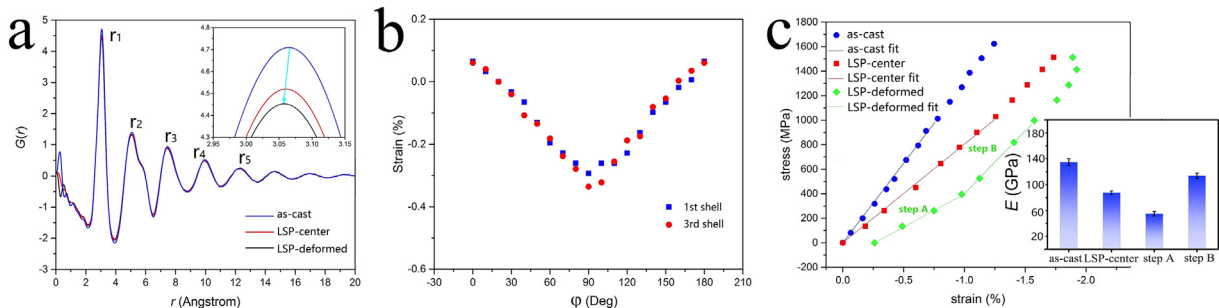


Fig. 2. (a) $G(r)$ of as-cast BMG, LSP-center and LSP-deformed. (b) Strain distribution of the 1st shell and 3rd shell of LSP-deformed. (c) Experiment and three-parameter viscoelastic model fit stress-strain results in the 1st shell of as-cast sample, LSP-center, and LSP-deformed zone respectively, the inset is the Young's modulus variation of 1st shell.

analyzed in atomic level. In last decades, Wang et al. [17–19] proposed dynamic flow unit model to describe the structural heterogeneity and to explain the mechanical behaviors of BMGs. The flow units are liquid-like zones with higher energy and lower elastic moduli in BMGs as compared to the surrounding elastic matrix [17,20–22]. We supposed that lots of flow units are induced by LSP and thus cause the lower E and perhaps the dual-step variation in compression tests. To prove such deduction, a three-parameter viscoelastic model based on Voigt model is used to simulate the viscoelastic deformation of the 1st shell in the LSPed BMG [17,23,24]. This model contains a spring (represents the elastic matrix) parallelly connected with a combination of a dashpot (represents the flow unit) and another spring (represents the shell of flow unit) in series. The governing equation for such a model is expressed as [17]:

$$E_2\sigma + \eta\frac{d\sigma}{dt} = E_1E_2\varepsilon + (E_1 + E_2)\eta\frac{d\varepsilon}{dt} \quad (3)$$

where σ is the applied stress and ε is the corresponding strain; E_1 , E_2 , and η are the modulus of elastic matrix, the modulus of flow unit shell, and the average viscosity of flow units, respectively (Fig. 3a). To avoid the shear instability in yielding stage which would disturb the model simulation, the experimental data used for the fitting are only those with $\sigma < 1000$ MPa [17,19,24]. The fitted stress-strain curves of the 1st shell are shown in Fig. 2c. The results suggest that the three-parameter model fits the experimental data very well. The fitting parameters of E_1 , E_2 , and η are listed in Table S1. E_1 is quite close to the E obtained by experiments (the inset of Fig. 2c), indicating that the elastic

matrix is the supporting component during compression. The η values are close to those of the super-cooled liquids and similar to literature results [17,21].

$\alpha = E_2/E_1$ is a factor that can be viewed as representing the total effect of the liquid-like flow units [17,19]. If α approaches zero, the BMG structure is fully constituted by elastic matrix which conforms elastic spring model; if α approaches infinity, the BMG is a completely liquid-like structure with broken elastic shells, thus the three-parameter model would degenerate to the Maxwell model [19]. The α and η values of different samples (and stress stages) are shown in Fig. 3b. Compared with the as-cast sample, higher α and lower η are shown in the step A of LSP-deformed zone. In the step B, however, α and η return to close to the as-cast and LSP-center at some extent. Such evolution of α and η values in LSP-deformed zone indicates that indeed a lot of atomic flow units with much lower activation energy [17] (than in the as-cast sample) were induced in 1st shell by LSP process, and these flow units were gradually reduced in compression test.

Previous studies [3,8,25] identified that the 1st shell exhibits the stiffest mechanical response whereas the high-order shells are progressively soft (Fig. S2a); as free volume enrichment zone, flow units are involved in high-order shells and they discretely distribute in metallic glasses, causing heterogeneities in atomic-structure and mechanical properties [17,20,21,24,26–29]. The atomic pairs in 1st shell usually has the least contribution to the flow units [8,30]. However, in this work, obvious atomic flow units with low η were induced in 1st shell of LSP-deformed zone (Figs. 2c and 3b). Combined with the atomic-structural homogenization revealed by similar E_s in 1st shell and 3rd shell, it can be deduced that a large number of flow units were induced

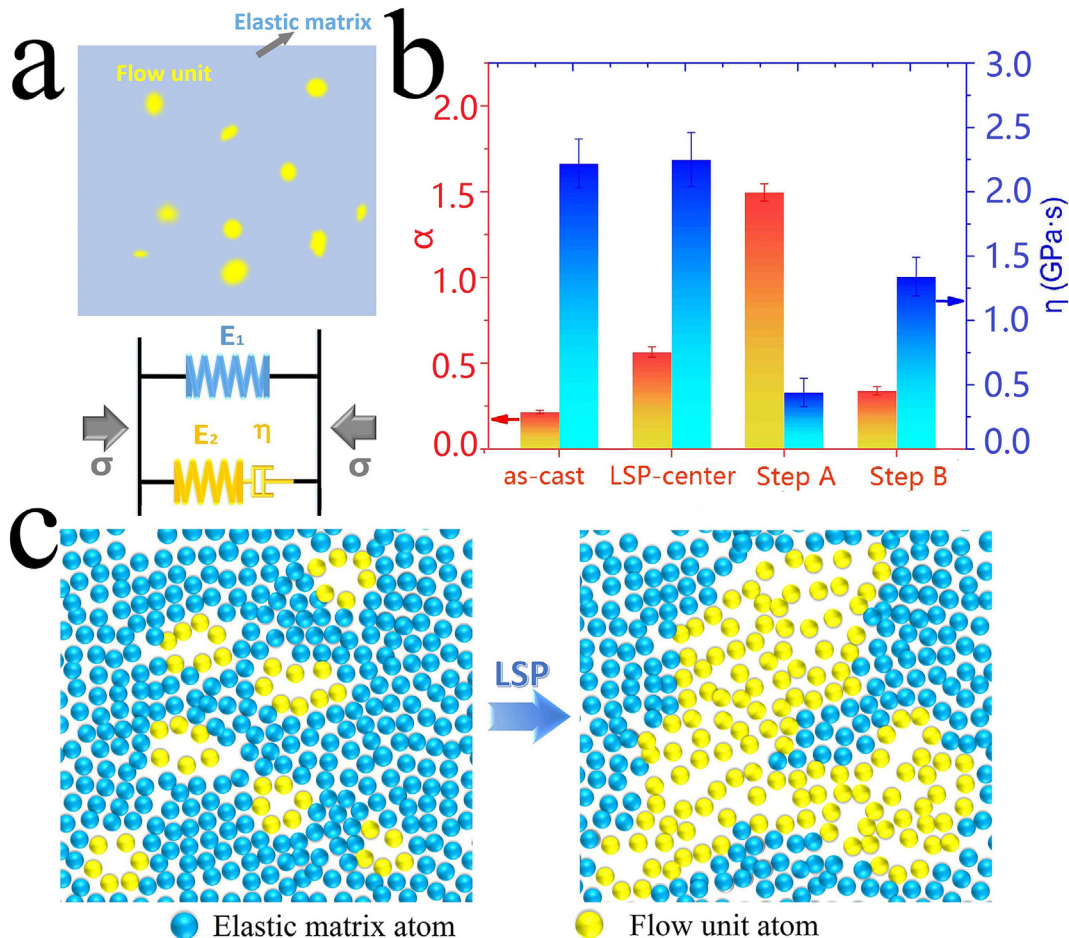


Fig. 3. (a) Schematic illustrations of the BMGs with flow units packaged by elastic matrix and three-parameter viscoelastic model for BMGs. (b) $\alpha = E_2/E_1$ and η variation with different samples. (c) The schematic of flow units generation after LSP.

in both 1st shell and high order shells, and these flow units were directly connected [17,31]. The flow unit generation is schematically shown in Fig. 3c.

How do the flow units connect with each other? It has been proven that flow units can be activated by external stress [32,33]. In convention loading mode, when the applied strain approaches yield, the adjacent regions around flow units are weak-bonded and easily transformed into a liquid-like state with much lower η , the flow units expand and the shear bands appear [34]. Since the flow units are softer than the elastic matrix, the stress tends to concentrate in the shear bands, inducing less stress on the matrix. The activation of new flow units in the matrix are terminated. During LSP process, the impact stress is calculated as ~ 18 GPa which is obviously much higher than the yield stress of BMGs, and the strain rate is higher than 10^6 s^{-1} [24,33]. During the impact, the structural heterogeneity is negligible and the whole impacted area will yield. A large number of flow units can be generated and expanded suddenly in both 1st shell and high order shells. High density flow units can thus be generated homogeneously. With the increase in the fraction of flow units, the percolation of flow units occurs and the flow units start to connect with each other (Fig. 3c). Eventually, local glass system would transform into a supercooled liquid state [20,35–37]. This evolution mechanism is similar to the thermally driven transition from glass to supercooled liquid. The interconnected flow units with low η homogenize the microstructure of the metallic glass and finally cause the E decrease.

In step B, flow units became fewer and atomic-structure re-hardened, suggesting a structure transformation. The atoms in flow units directionally flowed to accommodate the applied stress, and the atomic rearrangement was affected [38,39]. Therefore, atomic rearrangement analysis is necessary to understand the flow unit structure transformation from step A to step B. Atomic rearrangement could be characterized by the first coordination number (CN) [8]. CN is defined as the number of the nearest neighbor atoms around a central atom, and it can be determined as the area under the first peak of the radial distribution function (RDF) [4]:

$$\text{RDF}(r) = r \cdot G(r) + 4\pi r^2 \rho_0 \quad (4)$$

where ρ_0 is the average atomic number density. Fig. 4a shows the atomic packing variation for the LSP-deformed and the as-cast BMG versus the compressive stress along the loading direction. For the as-cast BMG, obvious linear variation of the atomic packing with the stress appears, and the final atomic packing variation is $\sim 3.2\%$. For the LSP-deformed zone, the atomic packing variation is $\sim 0.9\%$ when the applied stress is 0, showing that obvious atomic rearrangements are induced by LSP process, which is consistent with the results in Fig. 2b. In step A, the atomic packing variation rapidly increases to $\sim 2.8\%$; then, with the increase in the stress, the atomic packing variation is inconspicuous in step B and the final value is $\sim 3.4\%$.

During the elastic compression, atomic rearrangements can be generated with the applied stress increase. Some bonds are broken in the loading direction and some new bonds are formed in the transverse direction [8,39,40]. The atomic rearrangements usually vary linearly with the applied stress, causing linear atomic packing variation (Fig. 4a). Since amounts of interconnected flow units were generated in LSP-deformed zone, the atoms were loosely packed with low bonding energy [17–19]. These interconnected flow units were generally in high energy states and the microstructure was thus metastable. From a tensorial stress state point of view, it was found that an amorphous material has two kinds of localized defects: hydrostatic and shear stress field components [41]. De Hosson and colleagues [42–44] pointed out that the hydrostatic stress field component actually represents a free volume and can be annealed out by temperature or applied stress. Since the flow units are interconnected, free volume with hydrostatic stress field would be integrated such that this expanded hydrostatic stress field is unstable and easily affected by applied stress. In step A,

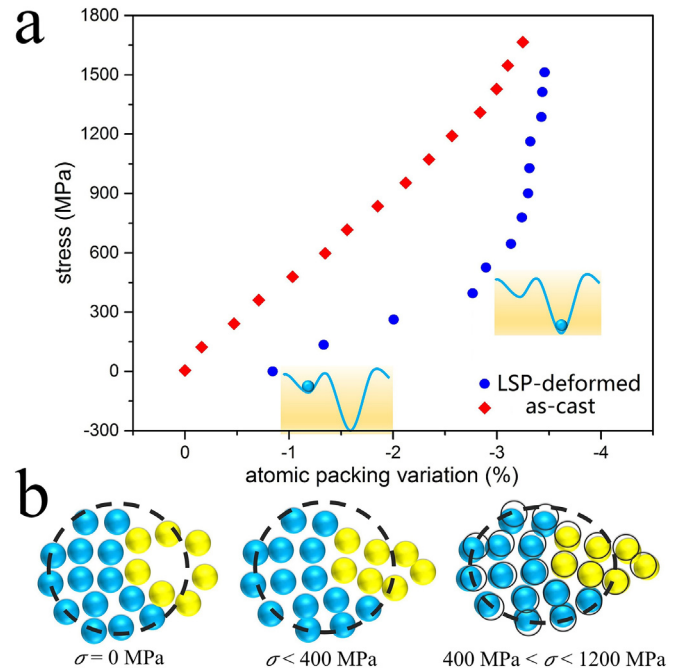


Fig. 4. (a) The atomic packing variation for the LSP-deformed and as-cast BMG versus compressive stress along the loading direction, insets are the potential energy landscape changes in the 1st elastic deformation step. (b) Schematic of the atomic-structure evolution in the LSP-deformed clusters during elastic compression.

external stress provides energy to surpass the energy barrier and activates the flow units, making atoms gradually rearrange to low energy states, and the structural relaxation appeared (Fig. 4b). With increasing applied stress, the hydrostatic stress field was broken up [41–44] and the atoms gradually compacted. The extra energy induced by LSP was then relaxed and the free volume in the flow units was annihilated. Such phenomenon is similar with the structure evolution in BMGs annealed at temperatures below glass transition temperature, T_g [33,45]. The inflection point $\sigma_i \sim 400$ MPa is a critical stress during the elastic compression, and it represents the highest energy barrier that atomic rearrangement needs. When the applied stress is higher than σ_i , the atoms were closely packed and few flow units existed in the atomic-structure. Therefore in step B, the volume fraction of flow units reduced and the η became even higher than in the as-cast BMG (Fig. 3b). The atomic rearrangement process became quite difficult and the atomic packing variation got smaller with the stress increase in step B (Fig. 4a). The elastic strain was mainly accommodated by the elastic compression of metallic bonds (Fig. 4b), causing the re-hardening (E increase) in step B.

Before closing, it needs to be noted that the flow unit annihilation here is mainly due to the atoms compaction caused by compressive stress. If the LSPed BMG was in tension, the tensile stress may promote the free volume expansion, thus the atomic-structure may keep a low E and have no flow unit annihilation. Moreover, it is also noteworthy that, while LSP induces flow units interconnection in the BMG, resulting in the higher density of shear bands and enhanced plasticity, one possible shortcoming of LSP technique may be that the low E in the LSPed region may cause a slight decrease in the fracture strength of BMG [9,10,46]. Further investigations in this field are desirable in future to push forward not only the understanding of flow unit interconnection but also its potential to improve the mechanical behavior of BMGs.

In summary, compared with linear strain variation in as-cast sample, a dual-step strain variation in LSPed BMGs was firstly found during compression tests by using in-situ HESXRD and PDF analysis. Structural heterogeneity between the 1st shell and high order shells in BMG was weakened after LSP, showing the atomic-structural homogenization. Flow unit model analysis reveals that LSP induced interconnected flow

units, which is responsible for the structural homogenization. Such interconnected flow units were metastable and thus annihilated during compression loading, causing the dual-step strain variation. We proposed that these metastable interconnected flow units achieve relatively fast relaxation at room temperature ($\sim 0.45T_g$) during compressive loading, providing a way to investigate the structure relaxation dynamics in experiments directly. It may also help to understand the correlation between atomic-structure and flow units, and to provide inspirations in improving the mechanical properties of BMGs.

This work was supported by the National Natural Science Foundation of China [Nos. 51471035 and 51701018]; Use of the Advanced Photon Source at Argonne National Laboratory was supported by U.S. Department of Energy [No. DE-AC02-06CH11357].

Appendix A. Supplementary data

Supplementary data to this article can be found online at <https://doi.org/10.1016/j.scriptamat.2018.02.019>.

References

- [1] A.L. Greer, *Science* 267 (1995) 1947–1953.
- [2] C.T. Liu, L. Heatherly, D.S. Easton, C.A. Carmichael, J.H. Schneibel, C.H. Chen, J.L. Wright, M.H. Yoo, J.A. Horton, A. Inoue, *Metall. Mater. Trans. A* 29 (1998) 1811–1820.
- [3] H.F. Poulsen, J.A. Wert, J. Neugefeind, V. Honkimaki, M. Daymond, *Nat. Mater.* 4 (2005) 33–36.
- [4] M. Stoica, J. Das, J. Bednarcik, H. Franz, N. Mattern, W.H. Wang, J. Eckert, *J. Appl. Phys.* 104 (2008) 13522.
- [5] G. Wang, N. Mattern, J. Bednarcik, R. Li, B. Zhang, J. Eckert, *Acta Mater.* 60 (2012) 3074–3083.
- [6] L.Y. Chen, B.Z. Li, X.D. Wang, F. Jiang, Y. Ren, P.K. Liaw, J.Z. Jiang, *Acta Mater.* 61 (2013) 1843–1850.
- [7] D.D. Qu, K.D. Liss, Y.J. Sun, M. Reid, J.D. Almer, K. Yan, Y.B. Wang, X.Z. Liao, J. Shen, *Acta Mater.* 61 (2013) 321–330.
- [8] H.S. Shahabi, S. Scudino, I. Kaban, M. Stoica, U. Rütt, U. Kühn, J. Eckert, *Acta Mater.* 95 (2015) 30–36.
- [9] Y. Cao, X. Xie, J. Antonaglia, B. Winiarski, G. Wang, Y.C. Shin, P.J. Withers, K.A. Dahmen, P.K. Liaw, *Sci. Rep.* 5 (2015) 10789.
- [10] J. Fu, Y. Zhu, C. Zheng, R. Liu, Z. Ji, *Appl. Surf. Sci.* 313 (2014) 692–697.
- [11] J. Fu, Y. Zhu, C. Zheng, R. Liu, Z. Ji, *Opt. Laser Technol.* 73 (2014) 94–100.
- [12] L. Wang, L. Wang, Z. Nie, Y. Ren, Y. Xue, R. Zhu, H. Zhang, H. Fu, *Mater. Des.* 111 (2016) 473–481.
- [13] L. Wang, L. Wang, Y. Xue, H. Zhang, H. Fu, *AIP Adv.* 5 (2015) 57156.
- [14] A.P. Hammersley, S.O. Svensson, M. Hanfland, A.N. Fitch, *High Pressure Res.* 14 (1996) 235–248.
- [15] I.K. Jeong, J. Thompson, T. Proffen, A.M.P. Turner, S.J.L. Billinge, *J. Appl. Crystallogr.* 34 (2001) 536.
- [16] W.H. Wang, *Prog. Mater. Sci.* 57 (2012) 487–656.
- [17] Z. Wang, P. Wen, L.S. Huo, H.Y. Bai, W.H. Wang, *Appl. Phys. Lett.* 101 (2012) 121906.
- [18] W. Jiao, B.A. Sun, P. Wen, H.Y. Bai, Q.P. Kong, W.H. Wang, *Appl. Phys. Lett.* 103 (2013) 81904.
- [19] L.S. Huo, J.F. Zeng, W.H. Wang, C.T. Liu, Y. Yang, *Acta Mater.* 61 (2013) 4329–4338.
- [20] Z. Lu, W. Jiao, W.H. Wang, H.Y. Bai, *Phys. Rev. Lett.* 113 (2014) 45501.
- [21] J.C. Ye, J. Lu, C.T. Liu, Q. Wang, Y. Yang, *Nat. Mater.* 9 (2010) 619–623.
- [22] X.J. Liu, Y. Xu, X. Hui, Z.P. Lu, F. Li, G.L. Chen, J. Lu, C.T. Liu, *Phys. Rev. Lett.* 105 (2010) 155501.
- [23] W. Jiao, P. Wen, H.L. Peng, H.Y. Bai, B.A. Sun, W.H. Wang, *Appl. Phys. Lett.* 102 (2013) 101903.
- [24] T.P. Ge, W.H. Wang, H.Y. Bai, *J. Appl. Phys.* 119 (2016) 204905.
- [25] H.W. Sheng, W.K. Luo, F.M. Alamgir, J.M. Bai, E. Ma, *Nature* 439 (2006) 419–425.
- [26] W. Dmowski, T. Iwashita, C.P. Chuang, J. Almer, T. Egami, *Phys. Rev. Lett.* 105 (2010), 205502.
- [27] Y. Yang, J.F. Zeng, A. Volland, J.J. Blandin, S. Gravier, C.T. Liu, *Acta Mater.* 60 (2012) 5260–5272.
- [28] L.S. Huo, J. Ma, H.B. Ke, H.Y. Bai, D.Q. Zhao, W.H. Wang, *J. Appl. Phys.* 111 (2012) 113522.
- [29] B.A. Sun, H.Y. Bai, Z. Wang, W.H. Wang, *Nat. Commun.* 5 (2014) 5823.
- [30] X. Bian, G. Wang, Q. Wang, B. Sun, I. Hussain, Q. Zhai, N. Mattern, J. Bednarcik, J. Eckert, *Mater. Res. Lett.* 5 (2017) 284–291.
- [31] Y. Yang, J.F. Zeng, J.C. Ye, J. Lu, *Appl. Phys. Lett.* 97 (2010) 261905.
- [32] Y.J. Wang, M. Zhang, L. Liu, S. Ogata, L.H. Dai, *Phys. Rev. B* 92 (2015) 174118.
- [33] T.P. Ge, X.Q. Gao, B. Huang, W.H. Wang, H.Y. Bai, *Intermetallics* 67 (2015) 47–51.
- [34] L.Z. Zhao, R.J. Xue, Y.Z. Li, W.H. Wang, H.Y. Bai, *J. Appl. Phys.* 118 (2015) 244901.
- [35] Y.C. Wu, B. Wang, Y.C. Hu, Z. Lu, Y.Z. Li, B.S. Shang, W.H. Wang, H.Y. Bai, P.F. Guan, *Scr. Mater.* 134 (2017) 75–79.
- [36] Z. Lu, X.N. Yang, B.A. Sun, Y.Z. Li, K. Chen, W.H. Wang, H.Y. Bai, *Scr. Mater.* 130 (2017) 229–233.
- [37] D.Z. Chen, C.Y. Shi, Q. An, Q. Zeng, W.L. Mao, *Science* 349 (2015) 1306.
- [38] N. Mattern, J. Bednarcik, S. Pauly, G. Wang, J. Das, J. Eckert, *Acta Mater.* 57 (2009) 4133–4139.
- [39] G. Wang, N. Mattern, S. Pauly, J. Bednarcik, J. Eckert, *Appl. Phys. Lett.* 95 (2009), 251906.
- [40] J. Das, M. Boström, N. Mattern, Å. Kvick, A. Yavari, A. Greer, J. Eckert, *Phys. Rev. B* 76 (2007), 92203.
- [41] V. Vitek, P.A. Warrendale, *Trans. Metall. Soc. AIME* 1983 (1983).
- [42] J.T.M. De Hosson, N.J.M. Carvalho, Y. Pei, D. Galvan, *Electron Microscopy Characterization of Nanostructured Coatings*, 2006.
- [43] Y.T. Pei, D. Galvan, J.T.M. De Hosson, *Acta Mater.* 53 (2005) 4505–4521.
- [44] J.R. Greer, J.T.M. De Hosson, *Prog. Mater. Sci.* 56 (2011) 654–724.
- [45] R.J. Xue, D.P. Wang, Z.G. Zhu, D.W. Ding, B. Zhang, W.H. Wang, *J. Appl. Phys.* 114 (2013) 123514.
- [46] M. Gao, J. Dong, Y. Huan, Y.T. Wang, W. Wang, *Sci. Rep.* 6 (2016) 21929.